Daniel Seidlitz, Emanuele Poliani, Maximilian Ries, Axel Hoffmann, Markus R. Wagner

Nanoscale InN clusters and compositional inhomogeneities in InGaN epitaxial layers quantified by tip-enhanced Raman scattering

Nanoscale InN clusters and compositional inhomogeneities in InGaN epitaxial layers quantified by tip-enhanced Raman scattering

D. Seidlitz, E. Poliani, M. Ries, A. Hoffmann, and M. R. Wagner*
Institute of Solid State Physics, Technische Universität Berlin, Hardenberstraße 36, 10623 Berlin, Germany
(Dated: April 1, 2021)

We investigate the compositional homogeneity of InGaN thin films with high In content grown by migration-enhanced plasma-assisted metal-organic chemical vapor deposition (MEPA-MOCVD). Micro-Raman spectroscopy and tip-enhanced Raman spectroscopy (TERS) are used to analyze the local InGaN composition on the micro- and nanoscale. Based on conventional micro-Raman mapping, the InGaN composition for all samples appears uniform but shows indications for intrinsic phase separations. TERS, a nanoscopic technique with a high spatial resolution far below the diffraction limit, verifies the formation of nanoscale compositional inhomogeneities. The dimensions of these compositional fluctuations observed in TERS are confirmed by scattering-type scanning near-field infrared nanoscopy (s-SNIN). In contrast to s-SNIN, we show that TERS furthermore enables the quantification of the In content in the different compositional regions and even allows the identification of InN nanoclusters near the surface of the epitaxial films.

Group III-nitride semiconductors are a well-proven material system for the fabrication of optoelectronic and photovoltaic devices. The ternary alloys InGaN and AlGaN enable simple engineering of the direct bandgap from the infrared (IR) to the ultraviolet (UV) region.[1] The bandgap range of InGaN includes the entire visible spectrum making it highly attractive as material in solid-state lighting sources such as light-emitting diodes (LEDs)[2] and laser diodes (LDs)[3] as well as multijunction solar cells.[4, 5] However, the growth of InGaN with high In content using conventional techniques like MOCVD and MBE encounters several challenges such as the large difference between growth temperature regions of InN and GaN due to their vastly different partial pressures[6] and the 11% lattice mismatch of InN and GaN.[7] Another difficulty is the formation of nanoscale lateral compositional inhomogeneities at the growth surface, thus reducing e.g. the surface and interface quality in heterostructures.[8, 9] In the case of InGaN, the group III atoms may segregate creating compositional inhomogeneities which can result in the formation of InN clusters.[9–11] Phase segregation is a mechanism caused by the deposition temperature and the lattice mismatch between InN and GaN, which results in a large miscibility gap.[12] Green LEDs based upon InGaN multi quantum wells (MQW) as active region are commercially available, but experience compositional inhomogeneities, thus leading to a reduced internal quantum efficiency with increasing In content (green gap).[13]

Raman spectroscopy is an established, non-destructive characterization method to investigate crystalline quality, compositional distribution, as well as strain and defects in e.g. InGaN films,[14, 15] quantum wells,[16] and quantum dots.[17] However, the resolution of Raman spectroscopy is not sufficient to investigate nanoscale inhomogeneities due to the diffraction limit. The study of phase separations on a nanometer scale requires nanoscopic characterization tools with a high spatial resolution far below the diffraction limit, e.g. near-field techniques. Tip-enhanced Raman scattering (TERS) combines micro-Raman spectroscopy with atomic force microscopy (AFM) thus reducing the scattering volume and enhancing the spatial resolution of Raman spectroscopy to the nm scale. Using TERS, we have previously observed InN segragation and polymorphism in InGaN/GaN multi quantum well nanorods.[18] Recently, we have demonstrated the impact of a resonant plasmonic interaction between the gold probe and the surface charge carriers in InN, which enhances the Raman scattering intensity and enables the detection of combinational second order Raman modes not accessible in conventional Raman spectroscopy.[19]

In this work, we present a nanoscale analysis and quantification of compositional fluctuations in InGaN thin films with high nominal In content between 26% and 92% grown by MEPA-MOCVD. The alloy compositions of all InGaN films appear highly homogeneous based on micro-Raman mapping. By contrast, TERS reveals the presence of compositional fluctuations and cluster formation on sub-diffraction length scales. We use these information to quantify the local In content and dimensions of the phase separations. The size of the phase separations determined by TERS is compared with results obtained by scattering-type scanning near-field infrared nanoscopy (s-SNIN) and found to be in excellent agreement.[20]

The InGaN films were grown epitaxially on c-plane sapphire templates using a low-pressure MEPA-MOCVD system. MEPA-MOCVD is an alternative approach to address the current growth challenges and fabricate In-rich InGaN alloys by kinetically stabilizing the InGaN growth surface.[20–22] In this approach, a tunable powered plasma source is mounted on top of a customized showerhead reactor. Nitrogen flows through the radio frequency (13.56 MHz) hollow cathode, which generates nitrogen reactive species (N*/NH*/NHx*) by plasma excitation and ionization. The dissociation of nitrogen by

* markus.wagner@physik.tu-berlin.de

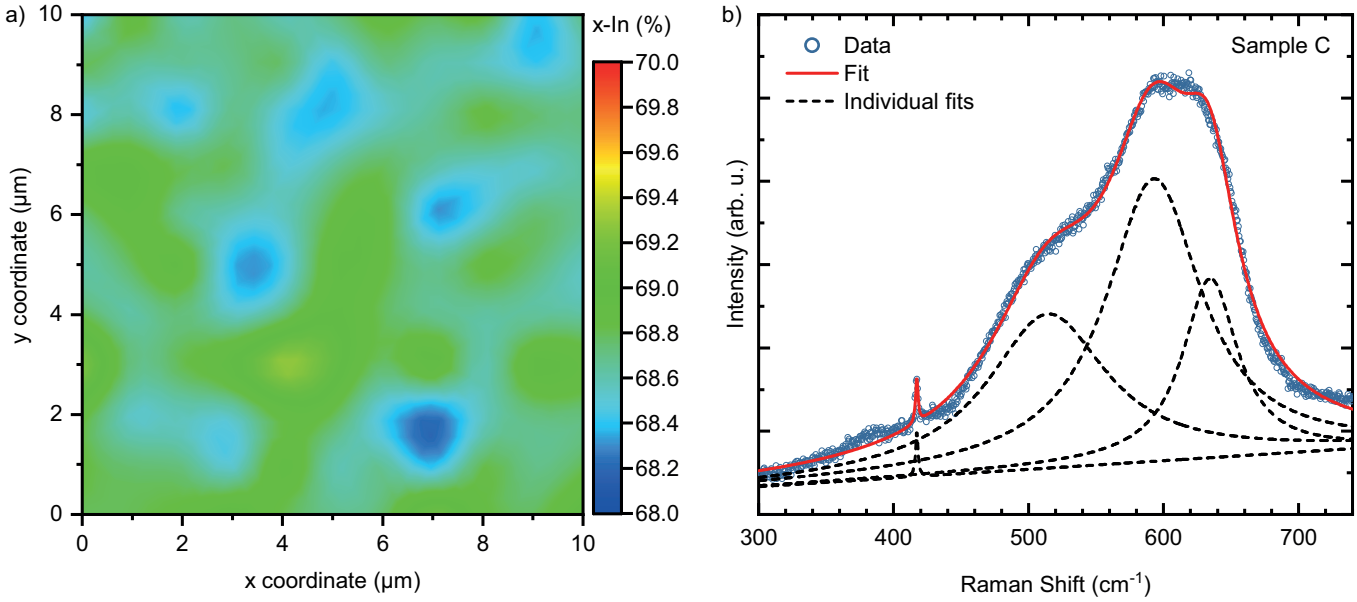

FIG. 1. (a) Spatial distribution of the In-concentration x in the $In_xGa_{1-x}N$ sample C, calculated from the InGaN A_1(LO) frequency shift using the MREI model. (b) An exemplary Raman spectrum at an arbitrary point of the map in (a). The blue circles are the experimental data, the red line is the fit function and the black lines are the single peak fits.

a hollow cathode is temperature independent in contrast to the dissociation of ammonia, which is used as nitrogen precursor in conventional MBE and MOCVD. The downstream of plasma-activated nitrogen species is directed to the growth surface where they interact with the group III metal atoms. The growth surface chemistry is stabilized by the kinetic energy provided by the excited nitrogen. As a result, desorption is suppressed, which leads to an increased diffusion time, and enhanced migration of the adatoms. The kinetics are a complex function of the growth parameters such as nitrogen flow through the plasma source and reactor pressure, as well as the composition and density of the plasma-excited nitrogen species, which can be tailored by the applied plasma power. In this work, the film deposition proceeded in an alternating pulse sequence of metalorganic (MO) precursor supply and nitrogen plasma exposure. Trimethylindium (TMI) and trimethylgallium (TMG) were injected simultaneously using nitrogen as the carrier gas. During the MO injection, the plasma power was set to 50 W to decrease the number of active nitrogen species, and therefore minimize possible counterproductive reactions between the MO and nitrogen precursors before they reach the growth surface. After the MO pulse, the growth surface was nitridated with a higher concentration of plasma nitrogen species using an increased plasma power of 400 W. The growth temperature was around 775C under a constant reactor pressure of 3.3 Torr. By variation of the TMI/TMG ratio, a set of In-rich $In_xGa_{1-x}N$ samples with $0.25<x<1$ were grown. A detailed description of the growth process parameters and initial characterization results can be found in reference.[20]

The micro-Raman scattering experiments were performed using a LabRAM HR-800 Raman setup by Horiba Jobin Yvon. The fully integrated system consists of a monochromator, a confocal microscope stage, and a cooled CCD-detector with a spectral resolution of better than 1 cm^{-1}. Two different laser excitation sources with emission wavelengths of 532 nm and 633 nm were used. The micro-Raman spectra were measured in backscattering geometry at room temperature using the 532 nm laser line. The setup for tip-enhanced Raman spectroscopy combines the Raman spectrometer with an AFM/STM Park XE-100 instrument. An 80x long-distance microscope focuses the 633 nm laser at an angle of 60° to the normal of the sample surface on the gold tip-surface cavity. This configuration allows excitation and detection of the tip-enhanced Raman scattering signal. The tip is produced by electrochemical etching of a 50 μm thick gold wire. The details of the TERS setup and scattering mechanisms are described in reference.[23]

TABLE I. Average $In_xGa_{1-x}N$ compositions evaluated from micro-Raman mapping (excitation 532 nm).

Sample	In-Composition x %	Deviation %	Thickness nm
A	26	± 0.5	43
B	46	± 1.0	44
C	69	± 1.0	85
D	86	± 0.5	86
E	92	± 0.5	86

The compositional homogeneity of the different InGaN films on the micrometer scale was studied by micro-Raman mapping over an area of 10×10 μm^2. The Raman

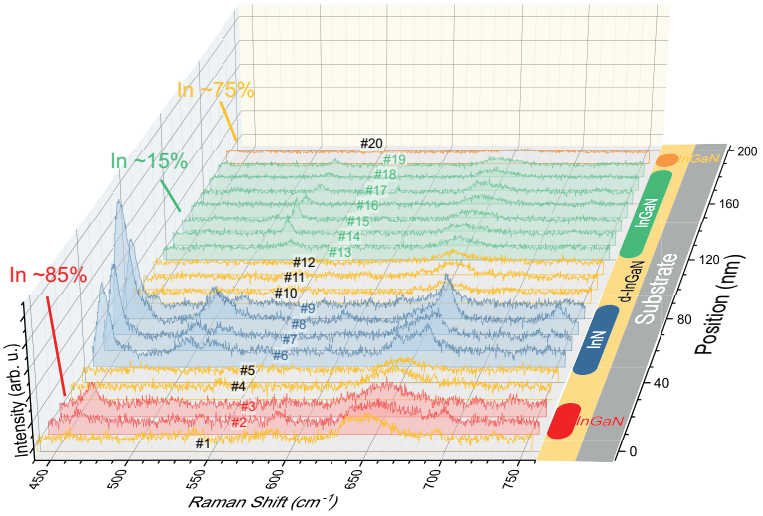

FIG. 2. TERS linescan of $In_xGa_{1-x}N$ (sample C, x=0.69) with step size of about 10 nm and excitation wavelength of 633 nm. Colors indicate domains of different In-content embedded in a disordered InGaN matrix. Exemplary spectra of each domain are displayed in Figure 3. On the right schematic illustration of the sample highlighting InN clusters and regions of different InGaN compositions correlated to the spectral position of the A_1(TO) mode.

spectra were recorded in 1 μm steps in x- and y-direction. The In-concentration were evaluated from the A_1(LO) phonon frequency shift. Based on the modified random iso-displacement (MREI) model,[24] the A_1(LO) phonon frequency shifts linearly as a function of the InGaN composition.[15, 25] In the exemplary Raman spectrum in Figure 1b, the A_1(LO) frequency around 634 cm^{-1} corresponds to an In-content of 69%. Analysis of each map spectrum provides a spatial-resolved distribution of the InGaN composition. Figure 1a on the left shows the spatial distribution of the In-percentage in the InGaN layer (sample C). The average In-percentage of the map is 69% with a deviation of less than ≈1%, indicating a high compositional homogeneity over the entire sample area. In general, all investigated samples appear to be very homogeneous when probed by diffraction limited micro-Raman spectroscopy, as listed in Table 1. The InGaN layer thickness is evaluated by FTIR spectroscopy.[26–28]

For an In-fraction of 69%, the MREI model predicts the E_2(high) phonon mode of InGaN around 514 cm^{-1}, which is in good agreement with the position of the unnamed peak at 513 cm^{-1} in Figure 1b. However, the large full width at half maximum (FWHM) of the peak is an indication of a significant degree of crystalline disorder. Furthermore, an additional peak at 592 cm^{-1} is observed in the Raman spectrum of sample C. This frequency coincides with the expected frequency of the A_1(LO) phonon mode of pure hexagonal InN and it suggests scattering from an ensemble of InN clusters. The coexistence of an InN (cluster) and an InGaN phase might be an indication of phase separation. The frequency of the additional peak at 592 cm^{-1} can also be related to the surface modes of InGaN due to the many interfaces between nanoclusters with different compositions.[29–31] Although the InGaN compositions of all samples appear to be very homogeneous, the strong broadening of the A_1(LO) modes is an indication for nanoscale compositional inhomogeneities that are inaccessible due to the spatial resolution of diffraction-limited probing techniques. As displayed in Figure 1b, the A_1(LO) of InGaN sample C has a FWHM of 49 cm^{-1}. Lateral compositional fluctuations at the growth surface are one of the major growth challenges for InGaN with high In content and can lead to bulk phase segregation and a reduction of the structural film quality. The characterization of these nanoscale phase separations requires optical near-field spectroscopic tools with a spatial resolution below the diffraction limit.

In order to investigate the InGaN film surface for possible nanoscale inhomogeneities, tip-enhanced Raman measurements were carried out. Figure 2 displays the TERS spectra obtained by a line scan along the surface of sample C with a total length of 200 nm and a step distance between adjacent spectra of about 10 nm. The scan direction is from spectrum #1 to #20. The experimental conditions of plasmon-resonant TERS lead to a strong near-field interaction between the plasmonic tip and the sample surface.[19] Therefore, several modes appear in the tip-enhanced Raman spectrum, which are imperceptible using far-field micro-Raman spectroscopy.

The analysis of the tip-enhanced Raman spectra allows to distinguish between regions of different $In_xGa_{1-x}N$ compositions and InN clusters. For clarification, individual colors highlight different domains corresponding to a distinct $In_xGa_{1-x}N$ composition. Numerical fitting of each TERS spectrum provides the phonon frequencies of the various Raman peaks. In the frequency range from 445 cm^{-1} to 530 cm^{-1}, strongly enhanced peaks are located at different positions. They are observed in each TERS spectrum. In the spectra #6-#9 of Figure 2, a phonon mode at 446 cm^{-1} is very dominant and shows

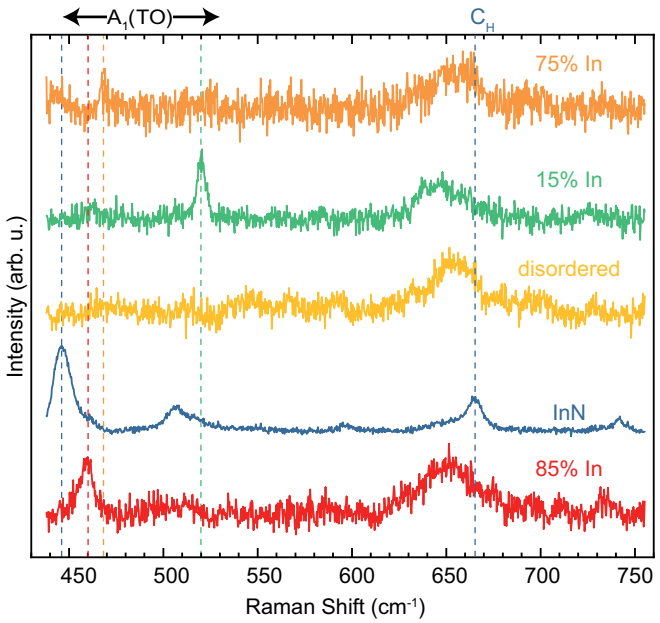

FIG. 3. Exemplary spectra of different $In_xGa_{1-x}N$ compositions as seen in the TERS line scan of Figure 2. Dashed lines highlight the A_1(TO) phonon modes of InN and different InGaN compositions as well as a feature C_H at 665 cm^{-1}.

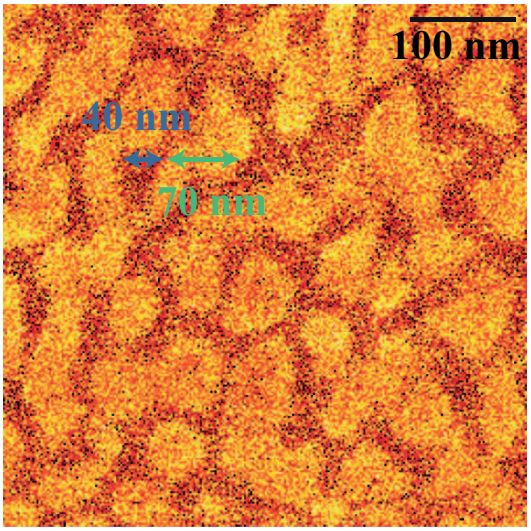

FIG. 4. S-SNIN image of $In_xGa_{1-x}N$ (sample C, x=0.69) taken at an excitation wavelength of $\lambda = 10.5$ μm showing nano-scale compositional fluctuations.[20] The dimensions of the phase separations indicated by arrows are in good agreement with the TERS results.

a strong enhancement in each spectrum. This frequency agrees well with the A_1(TO) phonon mode of InN,[32] identifying this area as an InN cluster. It should be noted that sapphire also has a Raman mode close to this frequency, but due to the layer thickness of 85 nm and the strongly confined probing-depth of TERS (5–10 nm), it can be excluded. Since the field density of the evanescent near-field at the tip decays exponentially, the spatial extent of the enhanced scattering volume is very small (<10 nm). Thus, TERS probes only a few nanometers into the surface and sapphire modes are no longer detectable.[23]

The spectra #2 and #3 show a tip-enhanced Raman peak located at 460 cm^{-1}. This peak is assigned to the A_1(TO) phonon mode of the InGaN alloy. The frequency shift of the A_1(TO) mode is converted into the In-concentration based on the MREI model[24] and corresponds to an In-concentration of 85%. Compared to the average In-content of 69% from Raman mapping, the In-fraction is 16% higher. The difference in the indium content is due to phase separations. Accumulation of In-atoms leads to the formation of In-clusters and In-rich InGaN regions resulting in an indium depletion of the surrounding matrix.[18] This agrees with the InGaN subset with a low In-content around 15%, highlighted by the green spectra #13-#19. The yellow spectra only show a broad feature around 650 cm^{-1} and lack distinct peaks that are necessary for the evaluation of the InGaN composition. These small areas are presumably disordered InGaN (d-InGaN). The correlation of the compositional information to the linescan step size combined with the tip-resolution enables a schematic illustration of the film surface structure as depicted on the right side of Figure 2. We note that a calculation of the In content based on the spectral position of the A_1(LO) instead of the A_1(TO) mode as conducted for the micro-Raman spectra is not possible for the TERS spectra due to the vanishing intensity of the A_1(LO) mode. This observation is in agreement with our previous works which do not show any A_1(TO) phonon modes in TERS spectra.[18, 19]. Moreover, the detection of the A_1(LO) is compounded by the fact that its spectral range coincides with the surface Raman modes in PR-TERS.

Figure 3 compares one exemplary tip-enhanced Raman spectrum of each of the five different domains from Figure 2. The dashed lines in Figure 3 mark the frequencies of the A_1(TO) mode for the different InGaN compositions. Furthermore, the tip-enhanced spectra corresponding to the InN cluster exhibit an additional feature at 665 cm^{-1}. This Raman shift does not match with any of the known far-field Raman modes of InN. Instead, this peak was recently observed in TERS of InN thin films and assigned to a two-phonon process involving the optical phonon mode A_1(TO) and the acoustic phonon M_H near the M-point of the Brillouin zone. The combinational mode of these two phonons is labeled C_H with a sum frequency of 663 cm^{-1}.[19] The strong enhancement of the second order phonon mode is caused by the plasmon-resonant excitation, i.e., resonance between the exciting photons, the localized surface plasmons (LSPs) and surface plasmon polaritons (SPPs) of the gold tip, and the locally increased free carrier density at the InN nanocluster at the surface of the InGaN layer.[19]

In order to support our analysis by an independent characterization technique, we compare the size of the

different $In_xGa_{1-x}N$ subsets as well as the InN clusters with previously published scattering-type scanning near-field infrared nanoscopy (s-SNIN) measurements of the same samples.[20] Figure 4 displays the acquired near-field amplitude image of sample C with an excitation wavelength of 10.5 μm.[20] The amplitude contrast identifies islands of different InGaN composition due to their different permittivity.[33] The results indicate phase separation in the InGaN alloys, which are due to spinodal decomposition.[9] In Figure 4, one can note brighter domains of a size which spans from 20 to 70 nm intercalated in a darker matrix with around 30 nm of mean size. In Figure 2, we detected three clusters by TERS with dimension of 20 nm, 40 nm and 70nm with A_1(TO) frequencies corresponding to In-contents of 80%, 100% and 75%, respectively. Those clusters alternate d-GaN of a dimension, which spans from 20 to 40 nm. The darker domains, detected by s-SNIN, likely correspond to high In-content clusters measured by TERS. Conversely, the brighter matrix probably corresponds to the intercalating d-GaN. Therefore, the dimensions of the nanoscale compositional fluctuations by TERS are in good agreement with the s-SNIN results indicated by the exemplary green and blue arrows in Figure 4.

The same characterization by micro-Raman spectroscopy and TERS was carried out also for Sample D, which has an average In-fraction of 86%. Comparable to the previously discussed case, conventional micro-Raman mapping of sample D shows a high compositional homogeneity. When measured by TERS, the sample reveals a reduced spatial homogeneity on the nanoscale. The line scan reported in Figure 5 consists of eight TERS spectra acquired with the same experimental conditions as described above. The scan direction goes from spectrum #1 to #8 with a step size of 40 nm. The spectra #6, #7, and #8 (blue) show two peaks at 447 cm^{-1} and 474 cm^{-1}. These peaks are in good agreement with the A_1(TO) and the E_1(TO) phonon modes of hexagonal InN, respectively.[32, 34] The spectra #1 and #2 (red) show an enhanced peak at 462 cm^{-1} which matches the energy of the A_1(TO) mode of InGaN. The frequency shift corresponds to an In-content of 80%, which is close to the average $In_{0.86}Ga_{0.14}N$ composition. The spectra #3, #4, and #5 are related to interstitial disordered $In_xGa_{1-x}N$. The separation of the InN and InGaN subsets by an area of disordered InGaN appears similar to the previously discussed results in sample C in Figure 2, however, the size of the different domains seems to be larger.

In agreement with sample C, we observe a mode located around 660 cm^{-1} in the In rich InGaN domains which is again attributed to the combinational mode C_H. The appearance of this mode in both InGaN samples with high In content is in alignment with the recently observed strong enhancement of second order modes in plasmon-resonant TERS (PR-TERS) of InN.[19] The combinational mode C_H also appears in spectrum #2 shifted equally with the A_1(TO) mode as expected.[19] In addition, a strongly enhanced peak at 500 cm^{-1} is visible in all cluster spectra, which cannot be assigned to the known far-field phonon modes of InN. This mode might be related to an accumulation of surface charges,[35] which is known to occur at InN surfaces.[36]

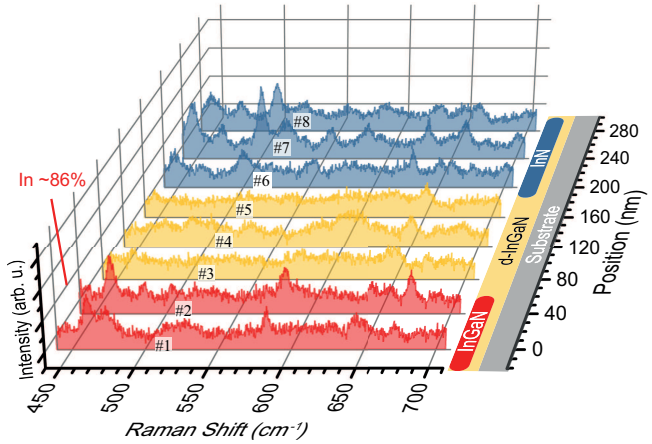

FIG. 5. TERS linescan of $In_xGa_{1-x}N$ (sample D, x=0.86) with step size 40 nm and excitation wavelength 633 nm. The graph colors represent the InN (blue), disordered $In_xGa_{1-x}N$ (yellow) and $In_{0.86}Ga_{0.14}N$ (red) areas.

In summary, In-rich InGaN films epitaxially grown by MEPA-MOCVD exhibit a very homogeneous alloy composition on a microscopic scale as confirmed by micro-Raman mapping experiments. The compositional fluctuations over an area of 10 × 10 μm are around 1% for each $In_xGa_{1-x}N$ sample based on the frequency shift of the A_1(LO) phonon. However, layers with an In-content x>0.4 exhibit indications for phase separations due to the broadening of the A_1(LO) phonon mode and the appearance of an InN A_1(LO) phonon. Investigations by TERS verified nanoscale compositional inhomogeneities at the surface of In-rich InGaN layers. The dimensions of these compositional fluctuations are in good agreement with previous results obtained by s-SNIN experiments. In contrast to s-SNIN, TERS provides quantification of the In-content x of the $In_xGa_{1-x}N$ phase separations based on the phonon frequency shift and even identifies InN nanocluster. The combinational modes C_L and C_H recently reported by plasmon-resonant TERS in InN are also detected in In-rich InGaN layers and contribute to the identification of InN nanoclusters.[19] The presence of these combinational modes is independent of the growth method and In content, which suggests that the plasmonic resonance condition is achievable in a large variety of InN based materials. The quantification of nanoscale compositional fluctuations and their corresponding dimensions by TERS in correlation with the process parameter space of MEPA-MOCVD can lead to a better understanding of the phase segregation mechanism to explore potential ways for its suppression and to form homogeneous InGaN structures with high In content.

The data that supports the findings of this study are available within the article.

[1] R. A. Ferreyra, C. Zhu, A. Teke, and H. Morkoç, Group iii nitrides, in *Springer Handbook of Electronic and Photonic Materials*, edited by S. Kasap and P. Capper (Springer International Publishing, Cham, 2017) p. 147.

[2] S. Nakamura, T. Mukai, and M. Senoh, Applied Physics Letters **64**, 1687 (1994).

[3] I. Akasaki and H. Amano, Japanese Journal of Applied Physics **45**, 9001 (2006).

[4] R. Dahal, J. Li, K. Aryal, J. Y. Lin, and H. X. Jiang, Applied Physics Letters **97**, 073115 (2010).

[5] D. V. P. McLaughlin and J. M. Pearce, Metallurgical and Materials Transactions A **44**, 1947 (2013).

[6] H.-J. Lewerenz and L. Peter, eds., *Photoelectrochemical Water Splitting* (Royal Society of Chemistry, 2013).

[7] H. Morkoç, *Handbook of Nitride Semiconductors and Devices* (Wiley, 2008).

[8] D. Doppalapudi, S. N. Basu, K. F. Ludwig, and T. D. Moustakas, Journal of Applied Physics **84**, 1389 (1998).

[9] C. Tessarek, S. Figge, T. Aschenbrenner, S. Bley, A. Rosenauer, M. Seyfried, J. Kalden, K. Sebald, J. Gutowski, and D. Hommel, Physical Review B **83**, 10.1103/physrevb.83.115316 (2011).

[10] H. Chen, R. M. Feenstra, J. E. Northrup, T. Zywietz, and J. Neugebauer, Physical Review Letters **85**, 1902 (2000).

[11] G. Stringfellow, Journal of Crystal Growth **312**, 735 (2010).

[12] I. hsiu Ho and G. B. Stringfellow, Applied Physics Letters **69**, 2701 (1996).

[13] M. A. der Maur, A. Pecchia, G. Penazzi, W. Rodrigues, and A. D. Carlo, Physical Review Letters **116**, 10.1103/physrevlett.116.027401 (2016).

[14] R. Oliva, J. Ibáñez, R. Cuscó, R. Kudrawiec, J. Serafinczuk, O. Martínez, J. Jiménez, M. Henini, C. Boney, A. Bensaoula, and L. Artús, Journal of Applied Physics **111**, 063502 (2012).

[15] S. Hernández, R. Cuscó, D. Pastor, L. Artús, K. P. O'Donnell, R. W. Martin, I. M. Watson, Y. Nanishi, and E. Calleja, Journal of Applied Physics **98**, 013511 (2005).

[16] S. Lazić, M. Moreno, J. M. Calleja, A. Trampert, K. H. Ploog, F. B. Naranjo, S. Fernandez, and E. Calleja, Applied Physics Letters **86**, 061905 (2005).

[17] V. Lemos, E. Silveira, J. R. Leite, A. Tabata, R. Trentin, L. M. R. Scolfaro, T. Frey, D. J. As, D. Schikora, and K. Lischka, Physical Review Letters **84**, 3666 (2000).

[18] E. Poliani, M. R. Wagner, J. S. Reparaz, M. Mandl, M. Strassburg, X. Kong, A. Trampert, C. M. S. Torres, A. Hoffmann, and J. Maultzsch, Nano Letters **13**, 3205 (2013).

[19] E. Poliani, D. Seidlitz, M. Ries, S. J. Choi, J. S. Speck, A. Hoffmann, and M. R. Wagner, The Journal of Physical Chemistry C **124**, 28178 (2020).

[20] D. Seidlitz, M. K. I. Senevirathna, Y. Abate, A. Hoffmann, and N. Dietz, in *Fourteenth International Conference on Solid State Lighting and LED-based Illumination Systems*, edited by M. H. Kane, J. Jiao, N. Dietz, and J.-J. Huang (SPIE, 2015).

[21] K. S. A. Butcher, D. Alexandrov, P. Terziyska, V. Georgiev, D. Georgieva, and P. W. Binsted, physica status solidi (a) **209**, 41 (2011).

[22] P. W. Binsted, K. S. A. Butcher, D. Alexandrov, P. Terziyska, D. Georgieva, R. Gergova, and V. Georgiev, MRS Proceedings **1396**, 10.1557/opl.2012.15 (2012).

[23] E. Poliani, M. R. Wagner, A. Vierck, F. Herziger, C. Nenstiel, F. Gannott, M. Schweiger, S. Fritze, A. Dadgar, J. Zaumseil, A. Krost, A. Hoffmann, and J. Maultzsch, The Journal of Physical Chemistry Letters **8**, 5462 (2017).

[24] H. Grille, C. Schnittler, and F. Bechstedt, Physical Review B **61**, 6091 (2000).

[25] D. Alexson, L. Bergman, R. J. Nemanich, M. Dutta, M. A. Stroscio, C. A. Parker, S. M. Bedair, N. A. El-Masry, and F. Adar, Journal of Applied Physics **89**, 798 (2001).

[26] N. Dietz, Materials Science and Engineering: B **87**, 1 (2001).

[27] Z. G. Hu, M. Strassburg, N. Dietz, A. G. U. Perera, A. Asghar, and I. T. Ferguson, Physical Review B **72**, 10.1103/physrevb.72.245326 (2005).

[28] M. K. I. Senevirathna, S. Gamage, R. Atalay, A. R. Acharya, A. G. U. Perera, N. Dietz, M. Buegler, A. Hoffmann, L. Su, A. Melton, and I. Ferguson, Journal of Vacuum Science & Technology A: Vacuum, Surfaces, and Films **30**, 031511 (2012).

[29] Y.-M. Chang, H. W. Chu, C.-H. Shen, and S. Gwo, Applied Physics Letters **90**, 072110 (2007).

[30] R. Mata, A. Cros, K. Hestroffer, and B. Daudin, Physical Review B **85**, 10.1103/physrevb.85.035322 (2012).

[31] E. Alarcón-Lladó, T. Brazzini, and J. W. Ager, Journal of Physics D: Applied Physics **49**, 255102 (2016).

[32] G. Kaczmarczyk, A. Kaschner, S. Reich, A. Hoffmann, C. Thomsen, D. J. As, A. P. Lima, D. Schikora, K. Lischka, R. Averbeck, and H. Riechert, Applied Physics Letters **76**, 2122 (2000).

[33] Y. Abate, D. Seidlitz, A. Fali, S. Gamage, V. Babicheva, V. S. Yakovlev, M. I. Stockman, R. Collazo, D. Alden, and N. Dietz, ACS Applied Materials & Interfaces **8**, 23160 (2016).

[34] J. S. Reparaz, K. P. da Silva, A. H. Romero, J. Serrano, M. R. Wagner, G. Callsen, S. J. Choi, J. S. Speck, and A. R. Goñi, Physical Review B **98**, 10.1103/physrevb.98.165204 (2018).

[35] K. K. Madapu, S. R. Polaki, and S. Dhara, Physical Chemistry Chemical Physics **18**, 18584 (2016).

[36] P. D. C. King, T. D. Veal, C. F. McConville, F. Fuchs, J. Furthmüller, F. Bechstedt, P. Schley, R. Goldhahn, J. Schörmann, D. J. As, K. Lischka, D. Muto, H. Naoi, Y. Nanishi, H. Lu, and W. J. Schaff, Applied Physics Letters **91**, 092101 (2007).